OPEN ACCESS

ACTA METALLURGICA SLOVACA

2025, VOL. 31, NO. 2, 124-128

SCICELL

RESEARCH PAPER

Influence of heat input on austenite/ferrite ratio in the weld zone of robotic GTAW duplex stainless steel 2205 weld bead

Bryan Ramiro Rodriguez-Vargas[1], Giulia Stornelli[1], Jorge Eduardo Hernandez-Flores[2,3], Emilia Imbimbo[1], Andrea Di Schino[1]*

[1] Università degli Studi di Perugia, Dipartimento di Ingegneria, Perugia, Italy

[2] InnovaBienestar de México, Ciencia y Tecnología 790, Fracc. Saltillo 400, 25290, Saltillo, Coahuila, Mexico

[3] Universidad Autónoma de Coahuila, Centro de Estudios e Investigaciones Interdisciplinarias, Arteaga, Coahuila, Mexico

*Corresponding author: giulia.stornelli@unipg.it, Università degli Studi di Perugia, Dipartimento di Ingegneria, Via Goffredo Duranti, 93, 06125 Perugia, Italy

Received: 08.04.2025
Accepted: 20.05.2025

ABSTRACT

This study analyzes the effect of Heat Input (HI) on the austenite/ferrite ratio in Duplex Stainless Steel (DSS) 2205 welds manufactured through the Robotic Gas Tungsten Arc Welding (GTAW) process using an Ar-2%N_2 shielding gas. Macrostructural and microstructural evaluations were performed to determine the effect of HI variations on weld bead geometry, phase balance and microhardness. The results indicate that, due to nitrogen desorption at higher temperatures, increasing HI leads to a reduction in austenite content. Lower HI promotes a higher austenite content, resulting in increased hardness. The study highlights the influence of nitrogen solubility and diffusion in the melt and demonstrates that shielding gas composition and welding parameters significantly affect the final microstructure and mechanical properties of DSS welds.

Keywords: Duplex Stainless Steel; Austenite-Ferrite ratio; Heat Input; Robotic GTAW

INTRODUCTION

Duplex Stainless Steel (DSS) gets its name from its stable two-phase microstructure at room temperature, resulting from the high content of alloying elements such as chromium and nickel. This microstructure is composed of roughly equal proportions of austenite (γ) and ferrite (δ), giving it a unique combination of mechanical properties and corrosion resistance [1–4]. Compared to austenitic stainless steels, DSS exhibit higher mechanical strength, allowing the design of lighter components without compromising structural integrity. They also exhibit excellent corrosion resistance, particularly in aggressive environments containing chlorides, allowing remarkable resistance to Pitting Corrosion and Stress Corrosion Cracking (SCC). This high mechanical strength, combined with good toughness, ductility and weldability, makes them suitable for several applications in the chemical, oil, marine and power generation industries [5–8].

Welding is an important process in the manufacture of DSS components for industries, as it allows the fabrication of structures with high mechanical strength and excellent corrosion performance. However, the choice of welding processes and the process parameters are critical factors in ensuring structural integrity and the desired material properties [9–13]. Among the most commonly used welding techniques for DSS are arc welding processes such as Gas Tungsten Arc Welding (GTAW). Its advantages include minimal post-cleaning and low heat input compared to other welding processes, allowing thin components to be joined [14, 15]. The thermal cycling during welding processes can induce changes in the microstructure of DSS, altering the two-phase ratio between ferrite and austenite. This phenomenon can create microstructural heterogeneities that negatively affect the mechanical properties and corrosion resistance of the material [16–19]. In addition to altering the phase ratio, high Heat Input (HI) can promote the precipitation of deleterious intermetallic compounds such as sigma phase (σ), chi phase (χ) and/or chromium nitrides (Cr_2N), which can form both in the weld zone (WZ) and the Heat-Affected Zone (HAZ) [20–22]. In contrast, if HI is too low, the cooling rate increases significantly, which can limit the formation of austenite in the WZ and therefore the microstructure can become predominantly ferritic, which negatively affects the toughness and ductility of the material [23, 24].

Therefore, the correct choice of welding parameters is a critical factor influencing the microstructural heterogeneity of the joint. At this regard, this study analyzes the effect of variation of the HI using an Ar-2%N shielding atmosphere on the austenite-ferrite ratio in the DSS 2205 weld bead by the Robotic GTAW process.

MATERIAL AND METHODS

DSS 2205 plate, 10 mm thick, was used as the base metal (BM) for the manufacture of the weld bead employing the filler metal ER2209. The chemical compositions of both the BM and filler metal are shown in **Table 1**.

Table 1. Chemical composition (wt.%) of BM and filler metal.

MATERIAL	CHEMICAL COMPOSITION						
	Fe	C	Cr	Ni	Mo	Si	N
DSS 2205	Bal.	0.02	22.8	7.0	2.84	0.26	0.19
ER 2209	Bal.	0.02	25.0-29.0	8.0-10.0	4.00	0.14	0.17

In order to investigate the effect of the HI on the weld metal, the BM was welded (bead-on-plate) by a fully automated GTAW. The welding parameters are present in **Table 2**.

Table 2. Welding operating parameters

SAMPLE	WELDING PARAMETERS				
	I (A)	V (V)	Welding speed ($mm \cdot s^{-1}$)	Wire feed speed ($mm \cdot min^{-1}$)	HI ($kJ \cdot mm^{-1}$)
Weld 1	230	12.6	200	1.7	1.1
Weld 2	230	12.6	202	1.7	0.87
Weld 3	180	12.6	165	1.4	0.82
Weld 4	180	12.6	150	1.4	0.79
Weld 5	180	12.6	130	1.4	0.59
Shielding gas: 98% Ar – 2% N_2 (12 L/min) Electrode: EWTh-2 (3.2 mm) Arc length: 1.2 mm					

HI was calculated according to Eq. (1). Given by the welding process the efficiency is assumed to be 60% (η).

$$HI = \eta \frac{I \cdot V}{S} \quad (1)$$

where HI is the Heat Input in $kJ \cdot mm^{-1}$, V is the welding voltage in Volts, I is the welding current in Amperes and S is the welding speed in $mm \cdot s^{-1}$.

The samples were prepared using conventional metallographic methods (in accordance with ASTM E3) [25] and electro-etched with nitric acid solution (50 ml HNO_3 + 50 ml H_2O) for 10 s at 6 V to evaluate macro and microstructural evolution. The macrostructure was inspected using a stereomicroscope (SM) (Nikon SMZ 745T) and the microstructure was characterized by optical microscope (OM) (Nikon Eclipse LV150). Quantification of austenite and ferrite fraction was performed by image analysis using a dedicated software (AlexaSoft, X-Plus, serial number: 6308919690486393, Florence, Italy). This analysis was

performed in 10 different fields and the reported values refer to the average of these measurements.

The hardness of the weld sample was measured using a microhardness tester (HXD-1000TM REMET, Remet, Bologna, Italy) with a 1 kg load. A cross-sectional profile of 15 indentations, spaced 1 mm apart, was made from the center of the WZ to the BM (**Fig. 1**).

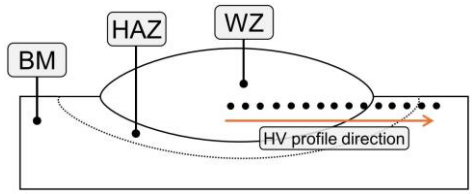

Fig. 1. Scheme of the HV profile

RESULTS AND DISCUSSION

Macrographs (**Fig. 2**) reveal a uniform weld structure with no visible discontinuities, such as undercuts, porosity, or hot cracks in the weld bead. However, the effect of HI can be seen in the different bead geometry, particularly when comparing Weld 1 and 5. **Fig.2(a)** shows that Weld 1 (high HI) has the greatest width (14.2 mm) compared to the other variants. This behavior is since a higher HI causes an increase in BM melting. In addition, the lower cooling rate associated with a high HI reduces the thermal gradients, which allows the melt to remain in the liquid state longer and increases the expansion of the weld pool prior to solidification. As the HI decreases, the bead width is reduced due to the lower energy available for BM fusion [20, 26]. This effect can be seen in Weld 5 (**Fig. 2(e))** where the lower HI limits the expansion of the weld pool and reduces the bead width to 10.2 mm. The decrease in HI also affects weld penetration. In the case of Weld 1, the higher penetration (3.0 mm) is favored compared to the other weld conditions (1.8 mm for Weld 5).

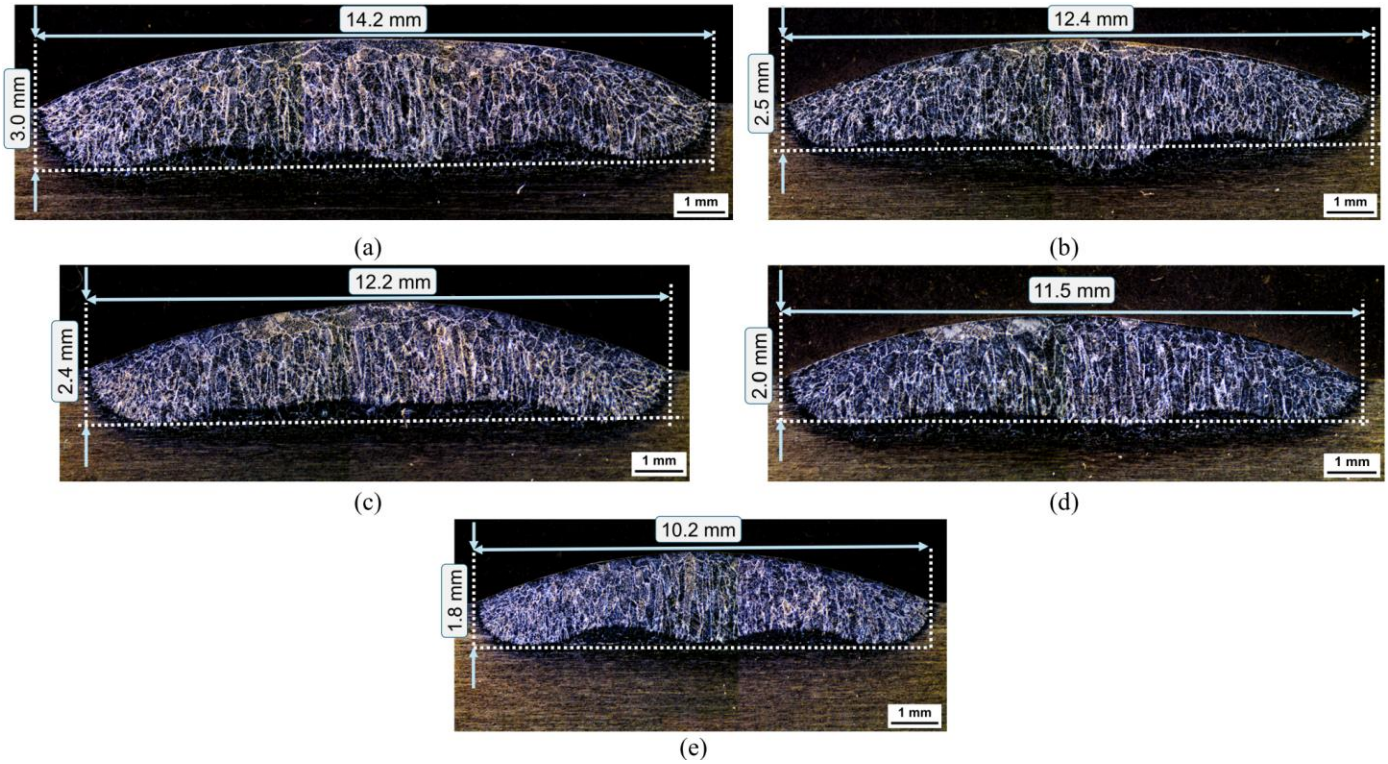

Fig. 2. Macrostructure of weld bead cross-sections with several HI conditions: (a) Weld 1 – 1.1 kJ·mm^{-1}; (b) Weld 2 – 0.87 kJ·mm^{-1}; (c) Weld 3 – 0.82 kJ·mm^{-1}; (d) Weld 4 – 0.79 kJ·mm^{-1}; (e) Weld 5 – 0.59 kJ·mm^{-1}

Fig. 3 illustrates the microstructural evolution in the WZ where four types of primary austenite morphologies are identified: Grain Boundary Austenite (GBA), Widmanstätten Austenite (WA), Intra-Granular Austenite (IGA) and Partially Transformed Austenite (PTA). These morphologies result from the transformation of ferrite to austenite during the solidification process, which is controlled by the diffusion of alloying elements such as nickel, nitrogen, among others [27, 28]. Although higher HI can reduce the solidification rate, which affects the weld bead geometry and the amount of γ phase, it does not significantly alter the nucleation and growth processes of several austenite morphologies within the ferritic matrix. This is clearly seen in **Fig. 3** where, although the weld macrostructure exhibits a qualitative change in the amount of austenite as a function of the HI variation, the microstructure of all variants exhibits the four austenite morphologies regardless of the HI values.

Table 3 shows the results of phase quantification in the weld as a function of HI. It can be observed that for a low value of HI (Weld 5 - 0.59 kJ/mm), the content of austenite in WZ is about 46%, while as the HI increases, the amount of austenite decreases to about 35%. It is important to note that although the content of this phase varies considerably with the change in HI, the use of a filler metal with a high nickel content (such as ER2209) contributes to the stabilization of austenite at room temperature, preventing its content from decreasing below 30% and ensuring adequate performance in most industrial applications [29].

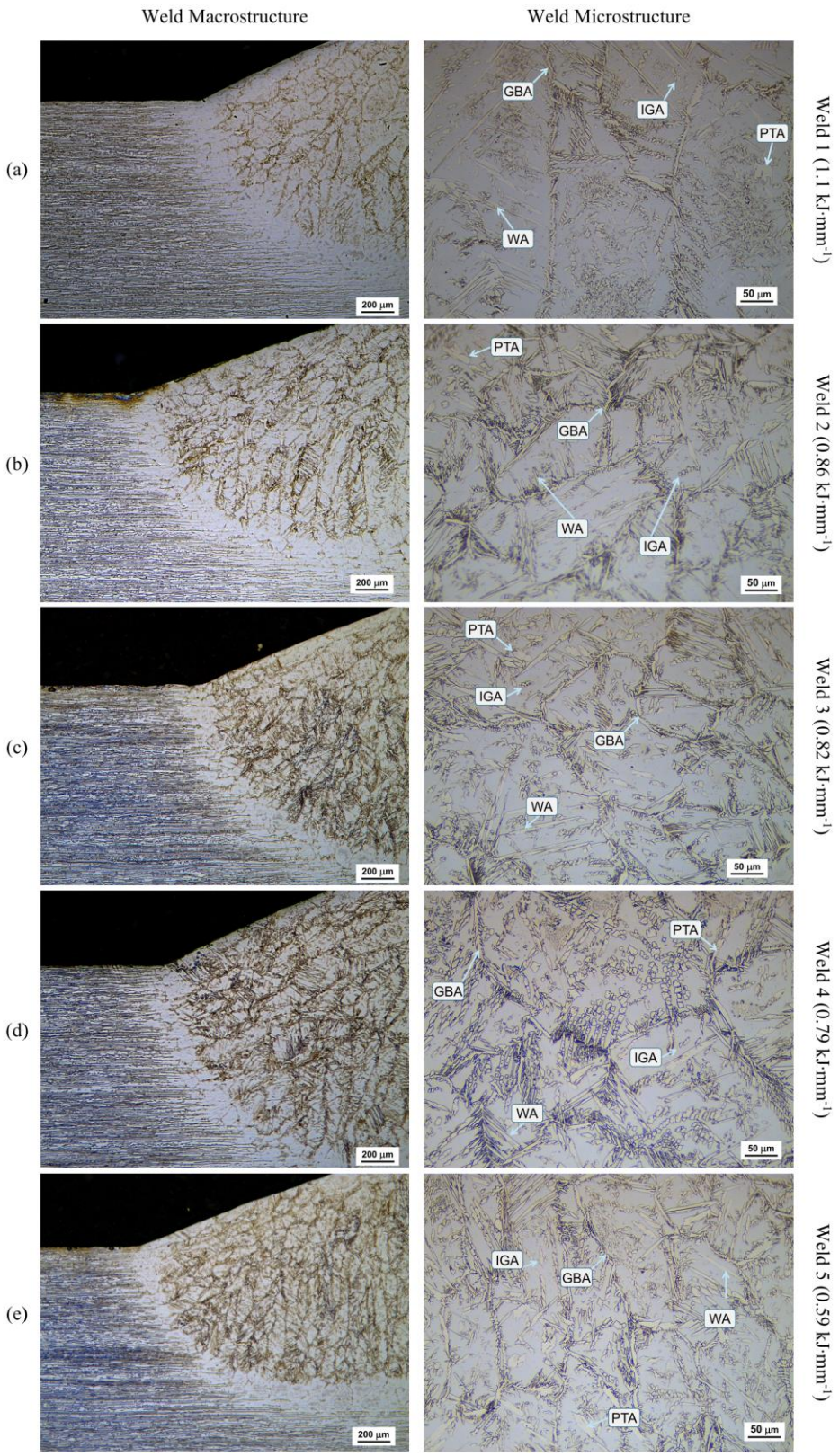

Fig. 3. Microstructural evolution of DSS weld bead with several HI conditions: (a) Weld 1 – 1.1 kJ·mm^{-1}; (b) Weld 2 – 0.87 kJ·mm^{-1}; (c) Weld 3 – 0.82 kJ·mm^{-1}; (d) Weld 4 – 0.79 kJ·mm^{-1}; (e) Weld 5 – 0.59 kJ·mm^{-1}

Table 3. Austenite/ferrite fraction and microhardness value through the DSS welding

SAMPLE	HI (kJ ·mm^{-1})	γ %	δ %	HV_1
Weld 1	1.1	34.3 ± 3.4	65.7 ± 3.1	278 ± 1.4
Weld 2	0.87	36.8 ± 3.9	63.2 ± 3.5	284 ± 1.0
Weld 3	0.82	37.9 ± 2.8	62.1 ± 3.4	285 ± 1.9
Weld 4	0.79	39.1 ± 3.1	60.9 ± 2.9	288 ± 1.5
Weld 5	0.52	46.8 ± 3.3	53.2 ± 3.7	295 ± 1.4

However, the reduction in austenite content with increasing HI contradicts the behavior generally expected in the welding of these materials, where an increase in HI reduces the cooling rate, promoting the diffusion and redistribution of austenite stabilizing elements, which would favor a higher proportion of this phase in the microstructure. The results obtained suggest that the relationship between HI and austenite proportion in WZ is not direct but is influenced by several interdependent factors. A key factor in this behavior is the influence of active gases (such as nitrogen) in the shielding gas. According to Sieverts' Law, the solubility of a gas in a liquid metal is proportional to the square root of its partial pressure in the surrounding atmosphere [30]. When pure argon shielding gas is used, the activity of nitrogen from the BM has practically no influence on the weld pool, so this element diffuses from the molten metal into the shielding gas. This results in a significant loss of nitrogen in the material and consequently less stabilization of the austenite. On the other hand, when using a shielding gas mixture with nitrogen, as in our investigation, its chemical activity in the gaseous atmosphere increases and an inverse diffusion gradient is established. This favors a consistent incorporation of nitrogen into the weld pool, which assists in the formation and stabilization of austenite [31]. However, the efficiency with which nitrogen is retained in the weld also depends on its solubility in the liquid/solid fraction of the weld pool. In the solid state, the crystalline structure allows the incorporation of nitrogen atoms into interstitial sites, which facilitates their retention and solubilization. In contrast, in the liquid state, the absence of an ordered structure facilitates the mobility of the atoms, reducing their solubilization and increasing their diffusion into the atmosphere [32, 33]. Since a higher HI increases the time that the weld pool remains in the liquid state, it also favors the desorption of nitrogen in the weld pool, which reduces its incorporation into the final microstructure. Therefore, although a nitrogen-enriched shielding gas favors its chemical activity in WZ, when the HI is high, the desorption loss may exceed the net absorption, resulting in a lower amount of retained nitrogen and, consequently, a reduction in the austenite content.

Fig. 4 shows the HV profiles for each weld, revealing a similar behavior across all variants: an increase in hardness in the HAZ and WZ compared to the BM. **Table 3** presents the average hardness values obtained from each profile. It can be observed that at lower HI, the hardness reaches values up to 295 HV_1, which coincides with a higher percentage of austenite in the microstructure. This behavior is a result of the interaction between the chemical composition and the phase distribution in the DSS weld. A determining factor in the hardening of the material is the amount of nitrogen in solid solution in the austenite [28, 35]. As mentioned above, the presence of this element in the interstitial position of the austenite causes lattice distortion and inhibits the movement of dislocations. As the nitrogen content in the austenite rises, the resistance to dislocation movement increases, raising both the hardness of this phase and the overall hardness of the weld.

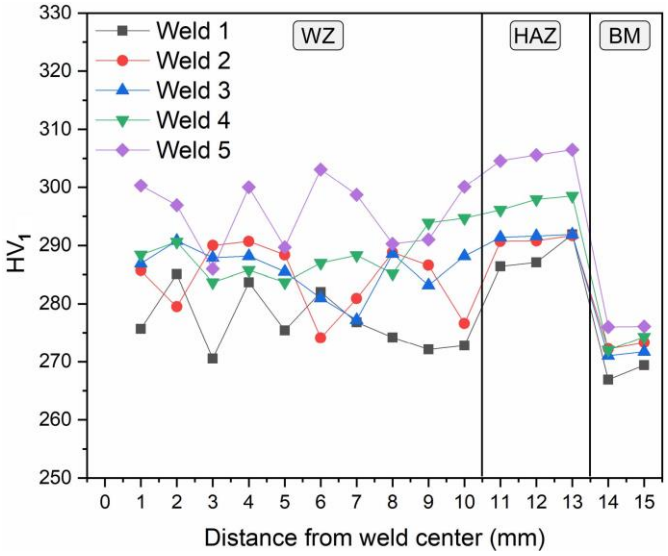

Fig. 4. Microhardness HV1 measurements in welds

CONCLUSIONS

This work presents the results of an investigation conducted to assess the influence of HI in weld bead of 2205 DSS plates using robotic GTAW process with Ar-2%N shielding atmosphere. The following conclusions summarize the findings:

- Heat input significantly affects the austenite/ferrite ratio in DSS 2205 welds. A lower HI results in a higher austenite content, while an increase in HI promotes a ferritic microstructure.
- Contrary to conventional weld zone behavior, higher HI results in a reduction of austenite content due to nitrogen desorption, which is influenced by shielding gas composition and diffusion kinetics.
- The use of a high nickel filler metal and Ar-2%N shielding gas helps to stabilize austenite; however, at higher HI, nitrogen loss limits its effectiveness in maintaining a balanced phases ratio.
- Weld metal hardness is directly related to austenite content, with lower HI conditions producing higher hardness values due to increased nitrogen retention in solid solution
- The use of bead-on-plate welds allows for precise control of HI and weld pool dynamics, enabling the tuning of phase balance and mechanical properties in 2205 DSS welds. This approach is especially relevant for analyzing microstructural evolution and hardness in applications where full penetration welds are not required.

REFERENCES

1. H. Yoon, H.-Y. Ha, S.-D. Kim, T.-H. Lee, J. H. Jang, J. Moon, N. Kang: Corrosion Science, 164, 2020, 108308. https://doi.org/10.1016/j.corsci.2019.108308
2. D. J. Lippold, J. C. Kotecki: *Welding Metallurgy and Weldability of Stainless Steels*. John Wiley & Sons, United States of America, 2005.
3. J. Kangazian and M. Shamanian: Journal of Manufacturing Processes, 26, 2017, 407-418. https://doi.org/10.1016/j.jmapro.2017.03.006
4. M.A. M, K.A. Shrikrishna, P. Sathiya, S. Goel: Journal of Manufacturing Processes, 18, 2015, 92-106. https://doi.org/10.1016/j.jmapro.2015.01.004
5. H. Luo, C.F. Dong, K. Xiao, X.G. Li: Applied Surface Science, 258, 2011, 631-639. https://doi.org/10.1016/j.apsusc.2011.06.077
6. K. Devendranath Ramkumar, D. Mishra, B. Ganesh Raj, M. K. Vignesh, G. Thiruvengatam, S. P. Sudharshan, N. Arivazhagan, N. Sivashanmugam, A. M. Rabel: Materials & Design, 66, 2015, 356-365. https://doi.org/10.1016/j.matdes.2014.10.084
7. L. Q. Guo, X. M. Zhao, M. Li, W. J. Zhang, Y. Bai, L. J. Qiao: Applied Surface Science, 259, 2012, 213-218. https://doi.org/10.1016/j.apsusc.2012.07.021
8. B. Ramiro Rodriguez Vargas, L. Albini, G. Tiracorrendo, R. Massi, G. Stornelli, A. Di Schino: Acta Metallurgica Slovaca, 29, 2023, 104-107. https://doi.org/10.36547/ams.29.2.1833
9. K. Bettahar, M. Bouabdallah, R. Badji, M. Gaceb, C. Kahloun, B. Bacroix: Materials & Design, 85, 2015, 221-229. https://doi.org/10.1016/j.matdes.2015.07.017

10. M. Yousefieh, M. Shamanian, A. Saatch: Journal of Iron and Steel Research International, 18, 2011, 65-69. https://doi.org/10.1016/S1006-706X(12)60036-3
11. Y. Yang, B. Yan, J. Li, J. Wang: Corrosion Science, 53, 2011, 3756-3763. https://doi.org/10.1016/j.corsci.2011.07.022
12. F. Veiga, A. Suárez, T. Artaza, E. Aldalur: Welding in the World, 66, 2022, 1081-1091. https://doi.org/10.1007/s40194-022-01295-4
13. R. Bidulsky, F.S. Gobber, J. Bidulska, M. Ceroni, T. Kvackaj, M.A. Grande: Metals, 11(11), 2021, 1831. https://doi.org/10.3390/met11111831
14. N. H. Manh, V. A. Nguyen, H. Le Duy, M. Akihisa, V. T. Le, T. Q. Ngoc, B. Gandham, Journal of Manufacturing Processes, 80, 2022, 683-691. https://doi.org/10.1016/j.jmapro.2022.06.043
15. M.H. Ngo, V.T. Le, B. Gandham, V.A. Nguyen, D.H. Le, T.N. Van: Journal of Manufacturing Processes, 85, 894-903. https://doi.org/10.1016/j.jmapro.2022.11.066
16. A. R. Pimenta, M. G. Diniz, G. Perez, I. G. Solórzano-Naranjo: Soldagem & Inspeção, 25, 2020. https://doi.org/10.1590/0104-9224/si25.12
17. K. H. Tseng, C. P. Chou, Journal of Materials Processing Technology, 123, 2002, 346-353. https://doi.org/10.1016/S0924-0136(02)00004-3
18. E. G. Betini, M. P. Gomes, C. S. Mucsi, M. T. D. Orlando, T. de S. Luz, M.-N. Avettand-Fènoël, J. L. Rossi: Materials Research, 22, 2019. https://doi.org/10.1590/1980-5373-mr-2019-0247
19. J. E. Hernandez-Flores, B. R. Rodriguez-Vargas, G. Stornelli, A. F. Miranda-Pérez, A. Di Schino, J. Gómez-Casas, F. de J. García-Vázquez: MRS Advances, 9, 2024, 1891-1895. https://doi.org/10.1557/s43580-024-00986-y
20. H. Tasalloti, P. Kah, J. Martikainen: Materials Characterization, 123, 2017, 29-41. https://doi.org/10.1016/j.matchar.2016.11.014
21. A. J. Ramirez, J. C. Lippold, S. D. Brandi: Metallurgical and Materials Transactions A, 34, 2003, 1575-1597. https://doi.org/10.1007/s11661-003-0304-9
22. G. Martin, S. K. Yerra, Y. Bréchet, M. Véron, J. D. Mithieux, B. Chéhab, L. Delannay, T. Pardoen: Acta Materialia, 60, 2012, 4646-4660. https://doi.org/10.1016/J.ACTAMAT.2012.03.040
23. A. F. Miranda-Pérez, B. R. Rodríguez-Vargas, I. Calliari, L. Pezzato: Materials 16, 2023. https://doi.org/10.3390/ma16051847
24. B. R. Rodriguez-Vargas, G. Stornelli, A. F. Miranda Pérez, A. Di Schino: Steel Research International, 95, 2024. https://doi.org/10.1002/srin.202300798
25. ASTM International, *Guide for Preparation of Metallographic Specimens*. 2017.
26. E. M. Westin, L. G. Westerberg: Welding in the World, 68, 2024, 1941-1063. https://doi.org/10.1007/s40194-024-01698-5
27. B. Gideon, L. Ward, G. Biddle: Journal of Minerals and Materials Characterization and Engineering, 07, 2008, 247-263. https://doi.org/10.4236/jmmce.2008.73019
28. Z. Zhang, H. Jing, L. Xu, Y. Han, L. Zhao, C. Zhou, Applied Surface Science, 404, 2017, 110-128. https://doi.org/10.1016/j.apsusc.2017.01.252
29. K. Trydell, K.-A. Persson, N. Fuertes, E. Siewert, N. Hussary, M. Pfreuntner, P. Bengtsson, P. Janiak, R. Vishnu, and M. Frodigh, Welding in the World, 67, 2023, 805-813. https://doi.org/10.1007/s40194-022-01447-6
30. S. Kou: *Welding Metallurgy*, John Wiley & Sons, Inc, United States of America, 2002.
31. L. Zhao, Z. Tian, Y. Peng, Y. Qi, Y. Wang: Journal of Iron and Steel Research, International, 14, 2007, 259-262. https://doi.org/10.1016/S1006-706X(08)60090-4
32. J. Y. Wang, T. Qi, C. L. Zhong, H. Zhang, X. R. Li, F. D. Liu: Optik, 242, 2021, 167026. https://doi.org/10.1016/j.ijleo.2021.167026
33. K. M. Hafez: The International Journal of Advanced Manufacturing Technology, 127, 2023, 1887-1894. https://doi.org/10.1007/s00170-023-11665-x
34. Z. Zhang, H. Jing, L. Xu, Y. Han, L. Zhao, J. Zhang: Applied Surface Science, 394, 2017, 297-314. https://doi.org/10.1016/j.apsusc.2016.10.047